Materialia 12 (2020) 100791

Contents lists available at ScienceDirect

Materialia

journal homepage: www.elsevier.com/locate/mtla

Ultra-thin intermetallic compound formation in microbump technology by the control of a low Zn concentration in solder

Yingxia Liu [a,*], Li Pu [a], Andriy Gusak [b], Xiuchen Zhao [a], Chengwen Tan [a], K.N. Tu [c]

[a] Department of Materials Science and Engineering, Beijing Institute of Technology, Beijing, China
[b] Department of Physics, Cherkasy National University, Ukraine
[c] Department of Materials Science and Engineering, University of California, Los Angeles, USA

ARTICLE INFO

Key words:
Lead-free solder
Diffusion
IMC growth kinetics
3D IC
Microbumps

ABSTRACT

We report here the extremely slow intermetallic compound (IMC) growth kinetics in the reflow reaction between a Sn-based solder of SnBiIn-2 at.% Zn and Cu. The solder has a melting point about 90 °C, and after reflow for 5 min on Cu at 120 °C, the formed IMC was Cu_5Zn_8 with a thickness only about 0.36 μm, which is much thinner than the IMC in nowaday packaging technologies. We systematically studied the IMC growth kinetics and built up a model to explain the extremely slow IMC growth rate. The growth kinetics of the reaction is non-parabolic and the activation energy is about 23.8 ± 1.6 kJ/mol. The non-parabolic kinetics is related to the lateral grain growth in IMC during the reactive diffusion along the moving grain boundaries. Our theoretical model shows that the growth rate of Cu_5Zn_8 compound should be proportional to the square root of Zn initial concentration in solder and a low Zn concentration in the solder will lead to a very slow IMC growth rate. The finding could be applied to control IMC thickness in 3D integrated circuit (3D IC) with micro-bump technology.

1. Introduction

As Moore's law of miniaturization in Si technology is approaching its physical and economic limit, 3D IC has been regarded as the most promising technology to sustain the law in the future [1–3]. 3D IC is achieved by stacking multiple chips using TSV (through-Si-via) and microbumps. There are three different size solder joints in the 3D architecture, including Ball Grid Array (about 760–200 μm), Controlled Collapse Chip Connection (C-4 joints about 100 μm) and microbumps (about 20 μm). In the future, the density of input/output connections in packaging will increase, so the size of μ-bump might be scaled down to 10 μm, 5 μm, or even only 1 μm [4–6]. This scaling trend will lead to serious reliability concerns and challenges in microbumps.

One of the main challenges is to control IMC thickness in microbumps. This is because the diameter of microbumps has been reduced more than 10 times from the C-4 joint, so the volume of solder will be reduced more than 1000 times [7]. Under the same reflow time, if we assume both the traditional solder balls and microbumps have the same IMC growth rate, the percentage of IMC would be much higher in microbumps. Furthermore, the IMC growth rate in small size solder bumps will be remarkably higher due to surface diffusion during interfacial reaction [8]. Actually, the solder layer in microbumps could transform completely into IMC after just aging for 24 h at 180 °C [9]. IMC is brittle in nature, and the high percentage of IMC will lead to the embrittlement problem in microbumps [10]. In addition, during IMC growth, solder layer will be experiencing volume shrinkage, and volume shrinkage works together with electromigration would lead to early failures [11–13]. Therefore, it's essential to control the IMC growth rate in the interfacial reaction between the solder and under bump metallization (UBM) in microbumps.

In this study, we report a Sn-Zn solder containing very low concentration of Zn solder that has an extremely slow reaction rate with Cu substrate. Some researchers have already investigated the effect of adding Zn to Sn-based solder to slow down the IMC growth kinetics [14–19]. However, the IMC growth rate in our work is much slower than the published results. Moreover, the reason of Zn effect to IMC growth kinetics is not systematically explained in those works, because Sn–Zn–Cu is a ternary system, and the reaction paths are complicated. Therefore, we developed a theoretical model for a systematic discussion of the competition among evolution paths in reactions between Cu with Sn-Zn solder. We explained that only a small amount of Zn can lead to the extremely slow reaction rate in IMC formation. The finding is important in the application of microbumps to advanced electronic packaging technology.

2. Experimental

SnBiIn-2 at.% Zn solder were prepared using high purity (>99.9%) Sn, Bi, In and Zn according to atomic ratio of Sn:Bi:In:Zn = 48:25:25:2. The ingots melted completely at around 300 °C in a vacuum induc-

* Corresponding author.
E-mail address: yingxia.liu@bit.edu.cn (Y. Liu).

https://doi.org/10.1016/j.mtla.2020.100791
Received 18 April 2020; Accepted 14 June 2020
Available online 16 June 2020
2589-1529/© 2020 Published by Elsevier B.V. on behalf of Acta Materialia Inc.

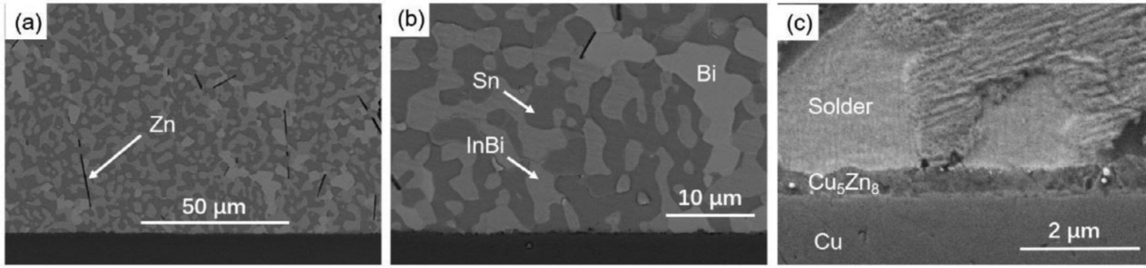

Fig. 1. The SEM graphic of interfacial microstructure after being reflowed for 10 min at 120 °C with different magnifications.

tion furnace under argon atmosphere. After smelting, the samples were cooled down to room temperature in air on a Cu substrate. Pieces about 5–10 mg were cut from the bulk solder alloy. We used differential thermal analysis (DTA) to measure the melting point of SnBiIn-2Zn solder. To study the wetting behavior, a piece of solder about 0.5 mg was placed on a Cu plate immersing in flux. Then we did reflow on a hot-plate at 120 °C, 140 °C and 160 °C for 5 min, 10 min, 30 min, 60 min and 120 min, respectively. After reflow, we cooled the samples in air to room temperature and cleaned the samples with pure alcohol.

The wetting samples were mounted in epoxy resin. We obtained the cross-sections by polishing with SiC papers successively and then with 0.04 μm SiO_2 powder suspension. We observed the cross-sections of the polished samples with scanning electron microscope (SEM). The top views of IMC grains were obtained by blowing away un-reacted liquid solder with high pressure gas during reflow, and were also observed by SEM. The elemental composition of IMC was analyzed by energy dispersive X-ray spectroscope (EDX). We measured the area and length of IMC by Image J. The thickness of IMC was obtained from area divided by length. The TEM sample was prepared by focus ion beam (FIB) using the in-situ FIB lift-out technique on an FEI G4 HX Dual Beam FIB/SEM. Transmission electron microscope (TEM) images were acquired by FEI Themis Z FEG/TEM operated at 200 kV in bright-field (BF) Scanning Tunneling Electron Microscopy (STEM) mode and by high-angle annular dark-field (HAADF) STEM mode for more detailed information.

Table 1
The thickness (μm) data of the IMC in the SnBiIn-2Zn/Cu samples.

Soldering condition	120 °C	140 °C	160 °C
5 min	0.366	0.438	0.425
10 min	0.464	0.495	0.558
30 min	0.577	0.760	0.887
60 min	0.773	1.048	1.277
120 min	0.890	1.302	1.735

3. Results

3.1. Interfacial microstructure

The melting point of the solder was measured by DTA to be 90 °C for SnBiIn-2 at.% Zn alloy. Fig. 1 shows the microstructure of solder after reflowing at 120 °C for 10 min and a layer of IMC has formed at the interface between solder and Cu. By back scattering electron (BSE) mode in SEM, four phases with different gray-level in the SnBiIn-2Zn solder matrix could be observed, as shown in Fig. 1(a) and (b). The phases are confirmed by both EDX and X-ray diffraction to be Sn-rich phase, Bi-rich phase, InBi phase, and needle-like Zn-rich phase. The white Bi phase is bigger than other phases and is easier to aggregate. Due to the low Zn content in the alloy, the dark needle-like Zn phase is much fewer and smaller than other phases. Fig. 1(c) shows the interfacial microstructure and the IMC with a layer-type morphology could be observed at the interface.

3.2. Growth kinetics of IMCs

The measured IMC thickness data of all the reflow samples are summarized in Table 1. Fig. 2 shows the cross-sectional SEM image of the IMC layer formed during the reflow reaction at 120 °C for different length of time (1 min, 5 min, 10 min, 30 min, 60 min and 120 min, respectively). Both Fig. 2 and the data measured in Table 1 show that the layer of IMC in the interface remains be the extremely thin, less than 1 μm, after reflow at 120 °C for 120 min. Even after reflow at 160 °C, which is 80 °C above the melting point of the solder alloy, for 120 min,

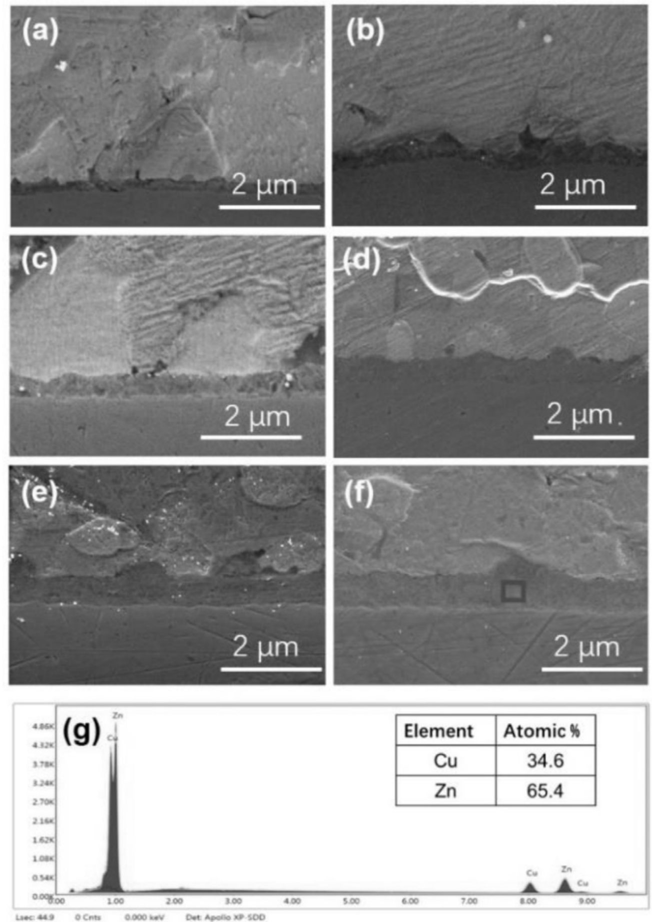

Fig. 2. (a) to Fig. 2(f). The cross-sectional SEM images (20,000X) of the interfacial microstructure of the SnBiIn-2Zn solder after reflowed at 120 °C for 1 min, 5 min, 10 min, 30 min, 60 min and 120 min; Fig. 2(g). The EDX results of IMC after being reflowed at 120 °C for 120 min.

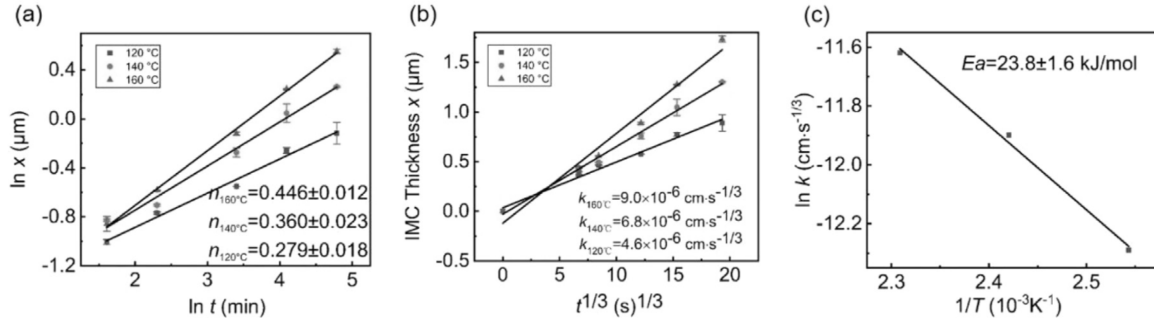

Fig. 3. (a). The plot by taking the logarithm on IMC thickness to ln t; Fig. 3(b). Measured IMC thickness plotted with $t^{1/3}$; and Fig. 3(c). Arrhenius-type plot of the growth rate constant to $1/T$.

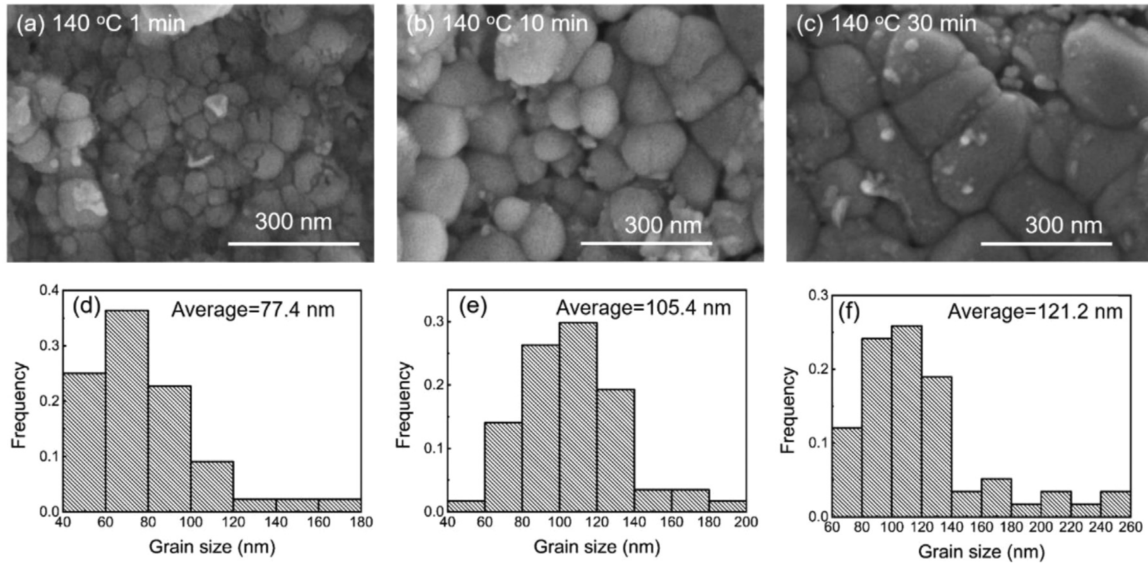

Fig. 4. The SEM images showing the top view of IMC grains formed in the SnBiIn-2Zn/Cu samples after reflow at 140 °C for 1 min (a), 10 min (b) and 30 min (c), respectively. Fig. 4(d)–(f). The frequency distribution of the grain size for the corresponding top view.

the IMC is still measured to be less than 2 μm. We are unable to obtain accurate IMC composition measurement by SEM-EDX for reflow time less than 30 min, since the IMC layer thickness is too thin. The composition of the IMC layer (indicated by the red triangular in Fig. 2) after reflow reaction at 120 °C for 60 min and 120 min is determined to be around 35 at.% Cu and 65 at.% Zn, as shown in Fig. 2(g), indicating that Cu_5Zn_8 is the dominate compound after the reaction.

According to Eq. (1) below,

$$x = kt^n \tag{1}$$

where x is the thickness of layer-type IMC, k is the growth rate constant and t is the reflow time. By fitting the measured thickness into Eq. (1) and taking the logarithm on both sides, we obtained the calculated n to be 0.279 ± 0.018, 0.360 ± 0.023 and 0.446 ± 0.012 for 120 °C, 140 °C and 160 °C, respectively, as shown in Fig. 3(a). Explanation of such time exponents was always a problem and still remains a problem. [20–22]. Therefore, alternative to Eq. (1), ways of approximation can be tried. In particular, taking into account low accuracy of time exponents determination, we may assume n to be 1/3 and optimize only the factor k in the empirical equation

$$x = kt^{\frac{1}{3}} \tag{2}$$

This type of dependence is well known for the growth kinetics of Cu_6Sn_5 phase in interactions of Cu with tin-based liquid solder [23,24]. The measured IMC thickness data is plotted to $t^{1/3}$ in Fig. 3(b). In Fig. 3(b), we can observe that all the linear correlation coefficient values (R) of the data obtained from three temperatures are bigger than 0.97, indicating the experimental results agree well with the empirical Eq. (2). The relationship implies the Cu_5Zn_8 IMC growth in this solder/Cu reaction can be ripening controlled.

The Arrhenius relationship can be used to calculate the activation energy for the Cu_5Zn_8 intermetallic compound growth

$$k = k_0 \exp\left(-\frac{Q}{RT}\right) \tag{3}$$

whereby k is a reaction constant and k_0 is a pre-factor, Q is the activation energy, R is the ideal gas constant, and T is the absolute temperature. The Arrhenius plots and fitting curve for our wetting samples are shown in Fig. 3(c) and the value of activation energy is calculated as 23.8 ± 1.6 kJ/mol.

3.3. Grain growth observation

We obtained the top views of IMCs by removing the un-reacted solder in order to have a direct observation of IMC grain growth. Fig. 4(a), 4(b) and 4(c) show the top view of the grain after the sample reflowed at 140 °C for 1 min, 10 min and 30 min, respectively. The corresponding IMC thickness of each sample is about 100 nm, 400–500 nm and 700–800 nm. We note that we were unable to get clear IMC top views by etching, because the IMC layer was too thin and it was hard to control the etching condition. Therefore, we adopted high pressure gas to blow the un-reacted liquid solder away directly during reflow. In this way, we

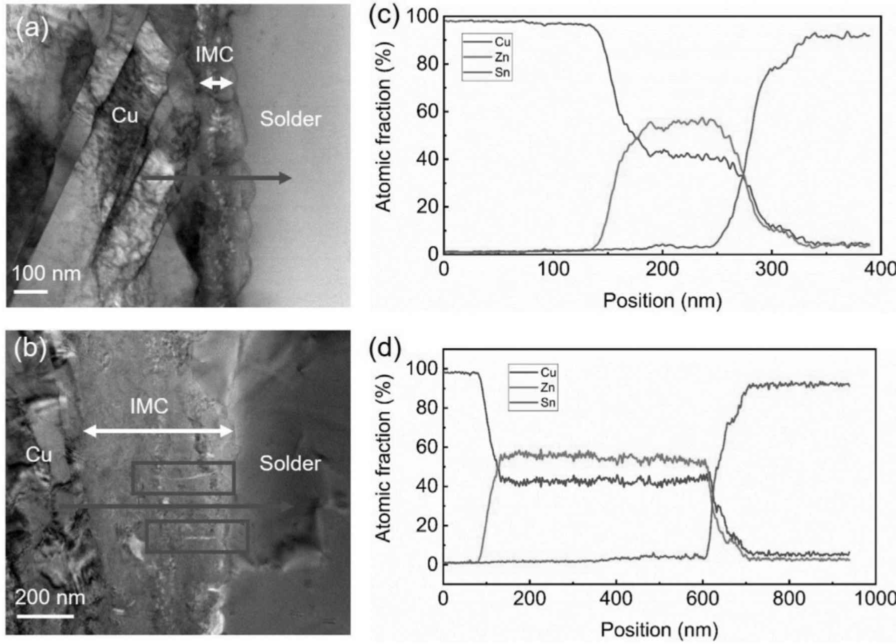

Fig. 5. (a) and (b). The STEM images of the sample after reflow at 140 °C for 1 min and 10 min, respectively; Fig 5. (c) and Fig 5. (d). The EDX line scan results in the corresponding STEM images.

can obtain a clear top view of grains, even though there is some dirt on the grains. Fig. 4(d)–(f) show the corresponding grain size distribution of those samples. The average grain size is about 77.4 nm, 105.4 nm and 121.2 nm for them, respectively. We can clearly observe the trend of grain growth in this set of images.

To have a clear investigation of IMC morphology and composition, we obtained STEM images of the IMC layer. Fig. 5(a) and (b) show the STEM images of the sample after reflow at 140 °C for 1 min and 10 min, respectively. Fig. 5(c) and (d) show the EDX line scan results in the corresponding STEM images. The red arrows mark the direction of line scan. Both the measured IMC compound is Cu_5Zn_8. In Fig. 5(a), the grain of IMC can be observed clearly. The grain has bump-type structure with size about 100 nm. In Fig. 5(b), the measured IMC thickness is consistent with the data listed in Table 1, around 450 nm. The grain is difficult to be distinguished in Fig. 5(b). We can observe some cracks between grains (marked in the red rectangular) and some tiny voids in the IMC. We are not sure about the formation reason of those voids currently. Those voids may be Kirkendall voids. Another possible reason is that the reflow temperature is only 140 °C and at this temperature, bubbles in flux might not be able to diffuse away, leaving those tiny voids on the interface of Cu and solder. Those voids are too small to hinder the reaction and should not affect much on our experiment.

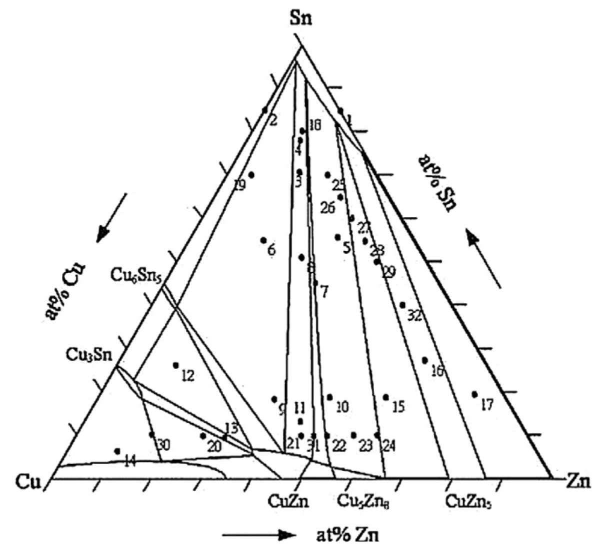

Fig. 6. Typical isothermal section of ternary phase diagram Cu–Sn–Zn.

4. Discussions

4.1. Kinetic model of reactions in Sn–Zn–Cu ternary system

Here we provide a systematical study on the slow growth kinetics of the IMC layer during the reaction between SnBiInZn solder and Cu substrate. The 5-component system of Cu–Sn–Zn–Bi-In is too complicated for theoretical analysis. Because we will treat mainly the formation of intermetallic phases on the basis of binary compounds of Cu_6Sn_5, CuZn, and Cu_5Zn_8, we will simplify our analysis by considering the ternary system of Cu-Sn-Zn, assuming that the role of Bi and In is in the reduction of eutectic temperature, but not the formation of new compounds in soldering reaction. To have some correspondence between the real 5-component system and the model of 3-component system, we will recalculate the real concentration, say, of Zn in 5-component system of $C_{Zn}=N_{Zn}/(N_{Cu}+N_{Sn}+N_{Zn}+N_{Bi}+N_{In})$ as $C_{ef\text{-}Zn}=C_{Zn}/(C_{Cu}+C_{Sn}+C_{Zn})$. In particular, 2 at.% of Zn in 4-component solder SnBiInZn corresponds to its effective concentration ($C_{ef\text{-}Zn}$) about 4 at.% in binary system Sn-Zn.

Fig. 6 is the typical isothermal section of ternary phase diagram Cu-Sn-Zn [25]. For our further analysis we will use even simpler model diagram with only 3 compounds (Cu_6Sn_5, CuZn, and Cu_5Zn_8) formation. Also, we will practically neglect the solubility of Sn in Cu-Zn phases, of Cu in Sn-Zn alloy, and of Zn in Cu-Sn phase. The simplified phase diagram is shown in Fig. 7. In Fig. 7, we marked three alternative diffusion paths: in the blue path, IMC CuZn (β) is formed in the reaction; in the black path, both CuZn (β) and Cu_5Zn_8 (γ) are formed; and in the red path, Cu_6Sn_5 (η) and CuZn (β) are formed.

We shall discuss the conditions for realization of various diffusion paths elsewhere (in separate long paper with full spectrum of possible regimes). In the experiment mentioned above, we observed, instead of the mentioned paths (a,b,c) at Fig. 7, another, fourth path: Cu-Cu_5Zn_8-(Sn+Zn). Evidently, this path does not correspond to the equilibrium diagram in Fig. 7 and means the kinetic suppression of the phase CuZn.

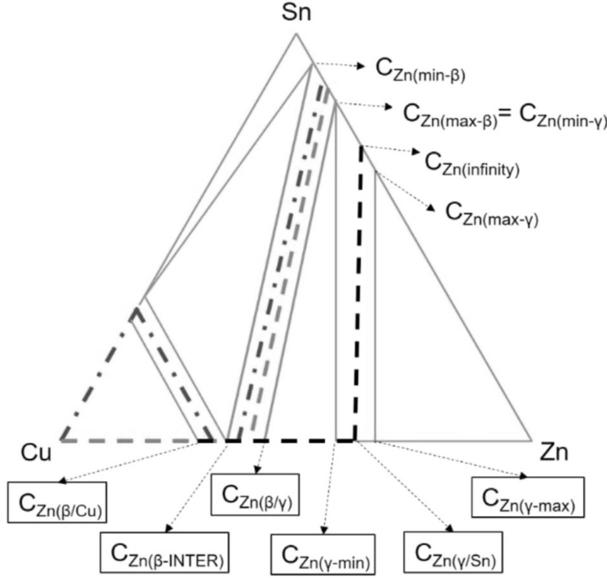

Fig. 7. Simplified phase diagram and three alternative diffusion paths: (a) Blue path, Cu-CuZn(β)-(Sn+Zn); (b) Black path, Cu-CuZn(β)-Cu_5Zn_8(γ)-(Sn+Zn); (c) Red path, Cu-Cu_6Sn_5(η)-CuZn(β)-(Sn+Zn).

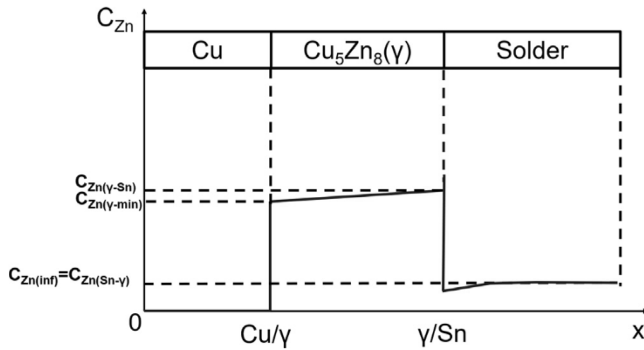

Fig. 8. Profile of Zn in case of single phase Cu_5Zn_8 phase growth.

This phenomenon is well-known in binary reactions Cu-Zn [26,27]. Ordered β-phase has much less interdiffusion coefficient than the first phase to grow (γ-phase Cu_5Zn_8). There exist at least two models explaining kinetic suppression [28,29].

Below we formulate the flux balance equations of the fluxes of Zn and Cu for the diffusion blue path (a) Cu-Cu_5Zn_8(γ)-(Sn+Zn) shown in Fig. 7, as if CuZn does not exist at all. The concentration profile of Zn in this case is shown in Fig. 8.

Profile at Fig. 8 would be strange in case of binary system. Yet, in ternary system the so-called "up-hill" flux across the interphase interface is case common – step of Zn concentration along the conode means the zero step of chemical potentials. So the flux of zinc is usual, "downhill" in respect to chemical potential.

Balance of Zn fluxes at boundary Cu/γ:

$$\left(C_{Zn}^{\gamma-\min}-0\right)\frac{dX^{Cu/\gamma}}{dt}=-D^{(\gamma)}\frac{C_{Zn}^{\gamma/Sn}-C_{Zn}^{\gamma-\min}}{\Delta X}-0 \tag{4}$$

Explicit zero in the left-hand side of Eq. (4) reminds that we neglect the solubility of Zn in Cu at low temperature. Explicit zero in the right-hand side of Eq. (4) reminds that we neglect the flux of Zn in the Cu matrix at the same low temperature. The explicit zeros in the following equations below have analogous meaning.

Balance equation of Cu fluxes at boundary Cu/γ, and this equation is equivalent to Eq. (4):

$$\left(\left(1-C_{Zn}^{\gamma-\min}\right)-1\right)\frac{dX^{Cu/\gamma}}{dt}=-D^{(\gamma)}\frac{\left(1-C_{Zn}^{\gamma/Sn}\right)-\left(1-C_{Zn}^{\gamma-\min}\right)}{\Delta X}-0 \tag{5}$$

Balance of Zn fluxes at boundary γ/Sn:

$$\left(C_{Zn}^{Sn/\gamma}-C_{Zn}^{\gamma/Sn}\right)\frac{dX^{\gamma/Sn}}{dt}=-D^{(solder)}\left.\frac{\partial C}{\partial x}\right|_{X(\gamma/Sn)+0}+D^{(\gamma)}\frac{C_{Zn}^{\gamma/Sn}-C_{Zn}^{\gamma-\min}}{\Delta X} \tag{6}$$

Balance of Cu fluxes at boundary γ/Sn:

$$\left(0-\left(1-C_{Zn}^{\gamma/Sn}\right)\right)\frac{dX^{\gamma/Sn}}{dt}=0-D^{(\gamma)}\frac{C_{Zn}^{\gamma/Sn}-C_{Zn}^{\gamma-\min}}{\Delta X} \tag{7}$$

Additional equation for this set is an approximate equation of conodes:

$$\frac{C_{Zn}^{Sn/\gamma}-C_{Zn}^{\min-\gamma}}{C_{Zn}^{\max-\gamma}-C_{Zn}^{\min-\gamma}}=\frac{C_{Zn}^{\gamma/Sn}-C_{Zn}^{\gamma-\min}}{C_{Zn}^{\gamma-\max}-C_{Zn}^{\gamma-\min}} \tag{8}$$

Now we make an important approximation: As we know, diffusivities in liquid are by several orders of magnitude higher than in solid. Therefore, we will formally assume that the interdiffusivity in molten solder, $D^{(solder)}=D_{liq}$ tends to infinity. (Indeed, typical diffusivity in melt, about $10^{-5}cm^2/s$, is much larger than even maximal diffusivities in solid at premelting temperature – about $10^{-8}cm^2/s$) Since the flux in the melt $-D^{(SnZn)}\frac{\partial C}{\partial x}$ cannot be infinite, it means that the concentration gradient of Zn in the melt should be zero, so that concentration at the boundary should be almost equal to concentration at "infinity". (Of course, it does not mean that flux itself it zero - it is a product of infinite diffusion coefficient times zero gradient and should be found from other equations.)

In Eq. (8) we take $C_{Zn}^{Sn/\gamma}\approx C_{Zn}^{Sn-\inf inity}$, so that

$$\frac{C_{Zn}^{Sn-\inf inity}-C_{Zn}^{\min-\gamma}}{C_{Zn}^{\max-\gamma}-C_{Zn}^{\min-\gamma}}=\frac{C_{Zn}^{\gamma/Sn}-C_{Zn}^{\gamma-\min}}{C_{Zn}^{\gamma-\max}-C_{Zn}^{\gamma-\min}} \tag{9}$$

and we will use Eq. (9) not for calculation of boundary velocity, but instead, for finding the indefinite Zn flux in molten solder, using the boundary velocity found from Eqs. (4) and (7), which we write in the form:

$$\frac{dX^{\gamma/Sn}}{dt}=\frac{1}{1-C_{Zn}^{\gamma/Sn}}D^{(\gamma)}\frac{C_{Zn}^{\gamma/Sn}-C_{Zn}^{\gamma-min}}{\Delta X}$$

$$\frac{dX^{Cu/\gamma}}{dt}=-\frac{1}{C_{Zn}^{\gamma-min}}D^{(\gamma)}\frac{C_{Zn}^{\gamma/Sn}-C_{Zn}^{\gamma-min}}{\Delta X}$$

Difference of these two equations gives:

$$\frac{d\Delta X^{\gamma}}{dt}=\left(\frac{1}{1-C_{Zn}^{\gamma/Sn}}+\frac{1}{C_{Zn}^{\gamma-\min}}\right)D^{(\gamma)}\frac{C_{Zn}^{\gamma/Sn}-C_{Zn}^{\gamma-\min}}{\Delta X}\approx$$
$$\approx\left(\frac{1}{5/13}+\frac{1}{8/13}\right)D^{(\gamma)}\frac{C_{Zn}^{\gamma/Sn}-C_{Zn}^{\gamma-\min}}{\Delta X}$$
$$\approx 4.2\cdot D^{(\gamma)}\frac{C_{Zn}^{\gamma/Sn}-C_{Zn}^{\gamma-\min}}{\Delta X} \tag{10}$$

Bulk diffusion via Cu_5Zn_8 at 250 °C and lower is almost frozen. On the other hand, most probably, Cu_5Zn_8 has no liquid channels between grains – otherwise it would grow for few microns in few minutes as Cu_6Sn_5 does in Cu-liquid Sn couple. So, most probably, the main mechanism of Cu_5Zn_8 layer is a grain-boundary diffusion along Cu_5Zn_8 grain boundaries (which may be grooved but without transformation into liquid channels).

Possibility 1. One can easily derive Eq. (2) for phase growth kinetics with time exponent 1/3 if one makes important and typical assumption:

we assume that the lateral grain size 2R of Cu_5Zn_8 growth with the layer thickness ΔX^γ and radius R is approximately equal to this layer thickness. Then the effective diffusivity across the layer is:

$$D^\gamma \approx \frac{\delta_{GB}}{R} D^\gamma_{GB} \approx \frac{\delta_{GB}}{\Delta X^\gamma} D^\gamma_{GB}. \tag{11}$$

Substitution of Eq. (11) into Eq. (10) gives:

$$\frac{d\Delta X}{dt} \approx 4.2\delta_{GB} D^{CuZn}_{GB} \frac{C^{\gamma/Sn}_{Zn} - C^{\gamma-min}_{Zn}}{(\Delta X)^2}. \tag{12}$$

Eq. (12) has an obvious solution with power law 1/3:

$$\Delta X^\gamma = \left(12.6 \cdot \delta_{GB} D^\gamma_{GB}\left(C^{\gamma/Sn}_{Zn} - C^{\gamma-min}_{Zn}\right)t^{1/3}\right). \tag{13}$$

Account of simplified conode Eq. (9) gives:

$$\Delta X^\gamma = \left(\frac{C^{Sn-\inf inity}_{Zn} - C^{\min-\gamma}_{Zn}}{C^{\max-\gamma}_{Zn} - C^{\min-\gamma}_{Zn}}\right)^{1/3} \left(12.6\delta_{GB} D^\gamma_{GB}\left(C^{\gamma-max}_{Zn} - C^{\gamma-min}_{Zn}\right)\right)t^{1/3} \tag{14}$$

From Eq. (12) one may see that the growth rate of the Cu_5Zn_8 compound satisfies the law 1/3 and is determined by the value $C^{Sn-\inf inity}_{Zn}$- concentration of Zn in Sn-based solution just before jump to about 50% in CuZn phase.

Possibility 2. .

One may try also an alternative way of approximation: we assume that the lateral grain size 2R of Cu_5Zn_8 grows with time as $R = At^m,\ m < 1$. So far, to the best of our knowledge, there is no generally accepted theory explaining time exponents different from 1/2. Qualitatively, non-parabolic grain growth is, most often, prescribed to solute drag or to Zener pinning by precipitates or voids. We don't know any theoretical model for lateral grain growth in the growing phase layer except [30,31]. Then the effective diffusivity across the layer is

$$D^\gamma \approx \frac{\delta_{GB}}{R} D^\gamma_{GB} \approx \frac{\delta_{GB}}{At^m} D^\gamma_{GB}. \tag{15}$$

Substitution of Eq. (15) into Eq. (10) gives:

$$(\Delta X)^1 d\Delta X \approx 4.2 \cdot \delta_{GB} D^\gamma_{GB}\left(C^{\gamma/Sn}_{Zn} - C^{\gamma-\min}_{Zn}\right)\frac{dt}{At^m}. \tag{16}$$

Eq. (16) has an obvious solution with power law (1-m)/2:

$$\Delta X = \left(\frac{8.4}{1-m}\frac{\delta_{GB} D^\gamma_{GB}}{A}\left(C^{\gamma/Sn}_{Zn} - C^{\gamma-\min}_{Zn}\right)\right)^{1/2} t^{\frac{1-m}{2}}. \tag{17}$$

Account of simplified conode Eq. (9) gives:

$$\Delta X = \left(\frac{8.4}{1-m}\frac{\delta_{GB} D^\gamma_{GB}}{A}\frac{C^{Sn-\inf inity}_{Zn} - C^{\min-\gamma}_{Zn}}{C^{\max-\gamma}_{Zn} - C^{\min-\gamma}_{Zn}}\left(C^{\gamma-\max}_{Zn} - C^{\gamma-\min}_{Zn}\right)\right)^{1/2} t^{\frac{1-m}{2}} \tag{18}$$

In case of normal lateral grain growth with $m = 1/2$, it should give $n = (1-1/2)/2 = 0.25$. In our experiments m is rather far from $\frac{1}{2}$. Using the data about lateral grain growth (77.4 nm, 105.4 nm and 121.2 nm after 1, 10 and 30 min), one can evaluate m as about 0.132. Possible explanation of such exponent for grain growth in the growing phase layer will be considered elsewhere. From Eq. (18) we may see that (within the Possibility 2) the growth rate of the Cu_5Zn_8 compound should satisfy the law $t^{0.43}$and is determined by the value $C^{Sn-\inf inity}_{Zn}$- concentration of Zn in Sn-based solution just before jump to Cu_5Zn_8 phase.

Possibility 3. .

Of course, with increasing temperature, the bulk diffusion across phase layer may play an increasing role (along with still important grain-boundary diffusion), so that the time exponent n for phase growth kinetics might approach $\frac{1}{2}$ with increasing temperature.

In all three possibilities 1, 2 and 3, the growth rate tends to zero (very slow growth) when $C^{Sn-\inf inity}_{Zn}$ tends to $C^{\min 2}_{Zn}$ (see Fig. 8). In reality, one would expect a more interesting picture: the growth rate of Cu_5Zn_8 decreasing will make the suppression of CuZn impossible, so that both phases (CuZn and Cu_5Zn_8) should appear.

In Section 4.1, lateral grain growth accompanying IMC growth, induced by reactive phase transformation at low temperature (frozen bulk diffusion), is analyzed. In many cases the reactive diffusion may proceed at low temperatures when bulk diffusion is practically frozen, yet the IMC phase growth proceeds via diffusion along grain boundaries as well as the lateral diffusion along interphase interfaces. In this case the regime may be related to the lateral grain growth in the IMC during the reactive diffusion along the moving grain boundaries. Based on this analysis, we built up the kinetic model and got Eqs. (14) and (18). We may see the growth rate of Cu_5Zn_8 should satisfy the law which varies from $t^{1/3}$ to $t^{0.43}$ and is determined by the concentration of Zn in Sn-based solution. As shown in Fig. 3(a), the measured n is 0.279 ± 0.018, 0.360 ± 0.023 and 0.446 ± 0.012 for 120, 140 and 160 °C reactions, which, in general, agrees with our kinetic model. Yet, the full theory taking into account the synergy of grain-boundary diffusion, bulk diffusion and of grain growth is still to be built.

4.2. The application of extremely slow IMC growth kinetics in electronic packaging

It should be noted the IMC growth kinetics is extremely slow in the reflow reaction between the SnBiIn-2%Zn solder and Cu. As shown in the TEM image, the thickness of the IMC is only 100 nm after reflow at 140 °C for 1 min. Even after reflow at 120 °C, which is 40 °C above the melting point of the solder alloy, for 120 min, the IMC is still less than 1 μm. There are many published studies on different IMCs growth kinetics in the reflow reaction. Among them, the most well-studied solder alloy in electronic packaging industry is SAC305. After reflowing for 1–3 min at a reflow temperature 40 °C above the melting points, the IMC is composed of Cu_6Sn_5 and Cu_3Sn, and the thickness is around 2–3 μm [32–34]. In comparison, the IMC thickness in SnBiIn-2%Zn solder is significantly thinner.

How to explain the slow reaction kinetics and to have a deeper understanding of the phenomenon is of interest. The measured activation energy in this work is 23.8 ± 1.6 kJ/mol. Some published data on the activation energy for solid-liquid interfacial reactions of Cu-Zn has been reported to be 26.4 ± 0.2 kJ/mol and 24.6 kJ/mol for Sn-8Zn-3Bi [35,36], 29.5 kJ/mol for SnZnIn [37] and 26 kJ/mol for Sn-9 Zn [38]. Our measured activation energy data is in the same range. In this way, the slow IMC growth rate could not be explained by the grain growth retarding resulted from the high percentage of Bi and In atoms in the alloy.

Our kinetic model actually can explain the slow IMC growth rate well. According to the model, the growth rate of Cu_5Zn_8 is determined by the concentration of Zn in Sn-based solution. In the alloy, the effective concentration of Zn in solder is about 4 at.%, leading to the suppression of CuZn and the formation of Cu_5Zn_8. However, the real concentration of Zn in the alloy is 2 at.%, much smaller than the Zn concentration when we observe Cu_5Zn_8 IMC formation in those reported works. For example, the Cu_5Zn_8 layer thickness is around 5 μm after reflow at 250 °C for 5 min, and the Zn concentration is eutectic Sn-Zn solder with 9 wt% (about 15 at.%) Zn [14,15]. Compared with our work, we can see that the small Zn percentage in our alloy can lead to the slow IMC growth kinetics. The low reflow temperature may also has some effects and makes the IMC growth rate even slower. Moreover, the depletion will shift Zn concentration closer to $C_{Zn(min\text{-}\gamma)}$ and even below it. The growth of IMC will become much slower when C_{Zn} approaches the $C_{Zn(min\text{-}\gamma)}$.

The slow IMC growth kinetics would be meaningful in advanced electronic packaging applications. If we apply SnBiIn-2Zn alloy to microbumps in 3D IC, the IMC thickness will be just 100–200 nm after one time reflow. The IMC growth and copper consumption in μ-bump could be controlled well this way. Nevertheless, the melting point of the reported solder is low and may have limited applications, we do find other SnBiIn-2Zn alloys with melting points higher than 140 °C but still very

slow IMC growth kinetics. By controlling Zn concentration in solder alloy, we can acquire a ten order of magnitude slower IMC growth rate compared with traditional solder. That is the key finding of this work and it would be of significance in the applications of advanced electronic packaging.

5. Conclusions

In conclusion, we reported the slow IMC growth kinetics in reflow reaction between SnBiIn-2%Zn solder and Cu substrate. After reflow for 5 min on Cu at 120 °C, the formed IMC is about 0.36 μm. The IMC growth activation energy is measured to be 23.8 ± 1.6 kJ/mol. The measured n in the relation of $x = kt^n$ is 0.279 ± 0.018, 0.360 ± 0.023 and 0.446 ± 0.012 for 120, 140 and 160 °C reactions, respectively.

A theoretical model based on the competition among possible reaction paths in the ternary system of Cu-Sn-Zn is presented to discuss the slow IMC growth kinetics. Our model shows that the growth rate of Cu_5Zn_8 should satisfy the law varies from $t^{1/3}$ to $t^{0.43}$ and is determined by the concentration of Zn in Sn-based solution.

In this way, a low Zn content in the solder will lead to a very slow growth rate. By controlling Zn concentration in solder alloy, we can acquire a ten order of magnitude slower IMC growth rate compared with traditional solder. The finding could be applied to control IMC thickness of microbumps in advanced electronic packaging technologies.

Declaration of Competing Interest

The authors declare that they have no known competing financial interests or personal relationships that could have appeared to influence the work reported in this paper.

Acknowledgements

The authors at Beijing Institute of Technology would like to acknowledge the financial support of "Youth Program of National Natural Science Foundation of China" with project number 51901022. The research of Andriy Gusak is supported by "Ministry of Education and Science of Ukraine" with project number 0118U003861.

Supplementary materials

Supplementary material associated with this article can be found, in the online version, at doi:10.1016/j.mtla.2020.100791.

References

[1] S. Gu, Material innovation opportunities for 3D integrated circuits from a wireless application point of view, MRS Bull. 40 (3) (2015) 233–241.
[2] Y. Liu, N. Tamura, D.W. Kim, S. Gu, K.N. Tu, A metastable phase of tin in 3D integrated circuit solder microbumps, Scr. Mater. 102 (2015) 39–42.
[3] W.R. Davis, J. Wilson, S. Mick, J. Xu, H. Hua, C. Mineo, A.M. Sule, M. Steer, P.D. Franzon, Demystifying 3D ICs, The pros and cons of going vertical, IEEE Des. Test Comput. 22 (6) (2005) 498–510.
[4] Y. Liu, M. Li, D.W. Kim, S. Gu, K.N. Tu, Synergistic effect of electromigration and Joule heating on system level weak-link failure in 2.5 D integrated circuits, J. Appl. Phys. 118 (13) (2015) 135304.
[5] H.Y. Hsiao, C.M. Liu, H.w. Lin, T.C. Liu, C.L. Lu, Y.S. Huang, C. Chen, K.N. Tu, Unidirectional growth of microbumps on (111)-oriented and nanotwinned copper, Science 336 (6084) (2012) 1007–1010.
[6] M. Huang, F. Yang, Size effect model on kinetics of interfacial reaction between Sn-xAg-yCu solders and Cu substrate, Sci. Rep. 4 (2014) 7117.
[7] K.N. Tu, Reliability challenges in 3D IC packaging technology, Microelectron. Reliab. 51 (3) (2011) 517–523.
[8] Y. Liu, Y.C. Chu, K.N. Tu, Scaling effect of interfacial reaction on intermetallic compound formation in Sn/Cu pillar down to 1 μm diameter, Acta Mater. 117 (2016) 146–152.
[9] S. Wang, L. Hsu, N. Wang, C. Ho, EBSD investigation of Cu-Sn IMC microstructural evolution in Cu/Sn-Ag/Cu microbumps during isothermal annealing, J. Electron. Mater. 43 (1) (2014) 219–228.
[10] Y. Wang, I.M. De Rosa, K.N. Tu, Size effect on ductile-to-brittle transition in Cu–solder-Cu micro-joints, in: 2015 IEEE 65th Electronic Components and Technology Conference (ECTC), IEEE, 2015, pp. 632–639.
[11] K. Son, G.T. Park, B.R. Lee, Y.B. Park, Volume shrinkage-induced voiding mechanism during electromigration of Cu/Ni/Sn-Ag microbump, J. Nanosci. Nanotechnol. 20 (1) (2020) 278–284.
[12] H.Y. Hsiao, J.K. Lin, Electromigration reliability and morphologies of Cu pillar with microbump under high current density stressing, in: 2015 IEEE 17th Electronics Packaging and Technology Conference (EPTC), IEEE, 2015, pp. 1–4.
[13] Y.W. Chang, C.C. Hu, H.Y. Peng, Y.C. Liang, C. Chen, T.C. Chang, C.J. Zhan, J.Y. Juang, A new failure mechanism of electromigration by surface diffusion of Sn on Ni and Cu metallization in microbumps, Sci. Rep. 8 (1) (2018) 5935.
[14] M. Islam, Y. Chan, M. Rizvi, W. Jillek, Investigations of interfacial reactions of Sn-Zn based and Sn-Ag-Cu lead-free solder alloys as replacement for Sn-Pb solder, J. Alloy. Compd. 400 (1–2) (2005) 136–144.
[15] K. Suganuma, K. Niihara, T. Shoutoku, Y Nakamura, Wetting and interface microstructure between Sn-Zn binary alloys and Cu, J. Mater. Res. 13 (10) (1998) 2859–2865.
[16] G. Zeng, S.D. McDonald, Q. Gu, Y. Terada, K. Uesugi, H. Yasuda, K. Nogita, The influence of Ni and Zn additions on microstructure and phase transformations in Sn-0.7 Cu/Cu solder joints, Acta Mater. 83 (2015) 357–371.
[17] F. Wang, X. Ma, Y. Qian, Improvement of microstructure and interface structure of eutectic Sn-0.7 Cu solder with small amount of Zn addition, Scr. Mater. 53 (6) (2005) 699–702.
[18] H.R. Kotadia, S.H. Mannan, A. Das, Influence of Zn concentration on interfacial intermetallics during liquid and solid state reaction of hypo and hypereutectic Sn-Zn solder alloys, J. Electron. Mater. 48 (5) (2019) 2731–2736.
[19] P.J.M. van der Straten, G.F. Bastin, F.J. van Loo, G.D. Rieck, Phase equilibria and interdiffusion in the cobalt-titanium system, Z. Metallkd. 67 (3) (1976) 152–157.
[20] H.H. Farrell, G.H. Gilmer, M. Suenaga, Grain boundary diffusion and growth of intermetallic layers: Nb3Sn, J. Appl. Phys. 45 (9) (1974) 4025–4035.
[21] G. Ghosh, Interfacial microstructure and the kinetics of interfacial reaction in diffusion couples between Sn-Pb solder and Cu/Ni/Pd metallization, Acta Mater. 48 (14) (2000) 3719–3738.
[22] A.M. Gusak, K.N. Tu, Kinetic theory of flux-driven ripening, Phys. Rev. B 66 (11) (2002) 115403.
[23] J.O. Suh, K.N. Tu, G.V. Lutsenko, A.M. Gusak, Size distribution and morphology of Cu_6Sn_5 scallops in wetting reaction between molten solder and copper, Acta Mater. 56 (5) (2008) 1075–1083.
[24] J. Zhou, Y. Sun, F. Xue, Properties of low melting point Sn-Zn-Bi solders, J. Alloy. Compd. 397 (1–2) (2005) 260–264.
[25] C.Y. Chou, S.W. Chen, Phase equilibria of the Sn-Zn-Cu ternary system, Acta Mater. 54 (9) (2006) 2393–2400.
[26] Y.E. Geguzin, Y.S. Kaganovskij, L. Paritskaya, V. Solunskij, Interphase boundary motion kinetics in mutual diffusion in two-component system, Fiz. Met. Metalloved. 47 (4) (1979) 821–833.
[27] I.E. Geguzin, The diffusion zone, Moscow Izdatel Nauka (1979).
[28] U. Gösele, K.N. Tu, Growth kinetics of planar binary diffusion couples: "Thin-film case" versus "bulk cases", J. Appl. Phys. 53 (4) (1982) 3252–3260.
[29] A. Gusak, K. Gurov, The kinetics of phase formation in the diffusion zone during interdiffusion. General theory, Fiz. Met. Metalloved. 53 (5) (1982) 842–847.
[30] K.N. Tu, A.M. Gusak, I. Sobchenko, Linear rate of grain growth in thin films during deposition, Phys. Rev. B 67 (24) (2003) 245408.
[31] A.M. Gusak, R. Abdank-Kozubski, D. Tyshchenko, Grain growth in open systems, in: Diffusion Foundations, 5, Trans Tech Publications Ltd, 2015, pp. 229–244.
[32] Y. Liu, S. Li, H. Zhang, H. Cai, F. Sun, G. Zhang, Microstructure and hardness of SAC305-xNi solder on Cu and graphene-coated Cu substrates, J. Mater. Sci. Mater. Electron. 29 (15) (2018) 13167–13175.
[33] W.Y. Chen, C.Y. Yu, J.G. Duh, Suppressing the growth of interfacial Cu-Sn intermetallic compounds in the Sn-3.0 Ag-0.5 Cu-0.1 Ni/Cu-15Zn solder joint during thermal aging, J. Mater. Sci. 47 (9) (2012) 4012–4018.
[34] M. Yang, Y.H. Ko, J. Bang, T.S. Kim, C.W. Lee, M. Li, Effects of Ag addition on solid-state interfacial reactions between Sn-Ag-Cu solder and Cu substrate, Mater. Charact. 124 (2017) 250–259.
[35] L. Liu, P. Wu, W. Zhou, Effects of Cu on the interfacial reactions between Sn-8Zn-3Bi-xCu solders and Cu substrate, Microelectron. Reliab. 54 (1) (2014) 259–264.
[36] W. Lin, T. Chuang, Interfacial reactions between liquid Sn-8Zn-3Bi solders and Cu substrates, J. Mater. Eng. Perform. 12 (4) (2003) 452–455.
[37] J. Pstruś, T. Gancarz, P. Fima, Effect of indium additions on the formation of interfacial intermetallic phases and the wettability at Sn-Zn-In/Cu interfaces, Adv. Mater. Sci. Eng. 2017 (2017).
[38] C. Lee, F. Shieu, Growth of intermetallic compounds in the Sn-9Zn/Cu joint, J. Electron. Mater. 35 (8) (2006) 1660–1664.